Rheology of granular mixtures with varying size, density, particle friction, and flow geometry

Eric C. P. Breard*
School of Geosciences, University of Edinburgh, Edinburgh EH8 9XP, United Kingdom and Department of Earth Sciences, University of Oregon, Eugene, Oregon 97403, USA

Luke Fullard†
Horizons Regional Council, Palmerston North 4410, New Zealand

Josef Dufek
Department of Earth Sciences, University of Oregon, Eugene, Oregon 97403, USA

(Received 11 August 2023; accepted 25 April 2024; published 22 May 2024)

Employing the discrete element method, we study the rheology of dense granular media, varying in size, density, and frictional properties of particles, across a spectrum from quasistatic to inertial regimes. By accounting for the volumetric contribution of each solid phase, we find that the stress ratio, μ, and concentration, ϕ, scale with the inertial number when using volume averaging to calculate mean particle density, friction, and size. Moreover, the critical packing fraction correlates with skewness, polydispersity, and particle friction, irrespective of the size distribution. Notably, following the work of Kim and Kamrin Phys. Rev. Lett. **125**, 088002 (2020), we introduce a rheological power-law scaling to collapse all our monodisperse and polydisperse data, reliant on concentration, dimensionless granular temperature, and the inertial number. This model seamlessly merges the $\mu(I)$-rheology and kinetic theory, enabling the unification of all local and nonlocal rheology data onto a single master curve.

DOI: 10.1103/PhysRevFluids.9.054303

I. BACKGROUND AND INTRODUCTION

Since granular flows are ubiquitous, understanding the flowing behavior of grains and powders has been increasingly necessary to predict hazards related to geophysical flows (e.g., snow avalanches [1], debris flows [2], rock avalanches [3], pyroclastic density currents [4–6], etc.) to understand processes on other planetary bodies (e.g., Mars [7] and Titan [8]), and to support applications in multibillion U.S. dollar industries and governmental agencies throughout the world [9] (e.g., pharmaceutical, agricultural, food industries, U.S. Departments of Energy and Defense). Granular flows have complex rheology; depending on particle shape, stiffness, friction, and size distribution, granular flows can display, for instance, history-dependent effects, hysteresis, nonlocality, dilatancy, and coupling with the interstitial fluid [9–11]. Numerous attempts have been made to build

*eric.breard@ed.ac.uk
†luke.fullard@horizons.govt.nz

constitutive models describing granular media, such as the $\mu(I)$-rheology that suggests a one-to-one relationship between the inertial number defined as $I \equiv \dot{\gamma}\bar{d}/\sqrt{P/\rho_s}$ and the shear-to-normal stress ratio defined as $\mu \equiv \tau/P$ [12–14], where τ is the shear stress, P is the normal stress, $\bar{d}$ is the mean particle diameter, $\dot{\gamma}$ is the shear rate, and ρ_s is the mean particle density. Most studies on granular flows focus on (quasi) monodisperse (single-particle size) and monophasic (e.g., [15]) mixtures of grains where all grains have the same frictional properties and densities, whereas natural mixtures can be made of particles with various densities and friction properties and are polydisperse (e.g., [16]). It is unclear at this time whether these complexities can be captured by a single rheological model [17]. In this work, we first investigate the rheology of granular flows in a simple shear setup using the discrete element method (DEM), and we perform simulations with monodisperse, polydisperse, and biphasic distributions (varying particle densities and particle-particle friction coefficients), thus expanding on the work of Gu *et al.* [18]. First, we demonstrate that the quasistatic, intermediate, and inertial-collisional regimes persist for all mixtures, wherein the solid concentration and stress ratio scale with the inertial number when taking into account the volumetric mean D_{43}. Second, following the recent work by Kim and Kamrin [19], we attempt to link the kinetic theory to the $\mu(I)$-rheology through the dimensionless granular temperature $\Theta \equiv \rho_s T/P$, where T is the granular temperature. Finally, we unify the rheology of the granular mixtures on various flow geometry using a modified power-law scaling $\mu(I, \Theta, \phi)$, demonstrating the need to account for the concentration to collapse our data on a master curve.

II. MATERIALS AND METHODS

A. Discrete element method

To simulate the granular flows in simple shear, we used the open-source code MFIX developed by the U.S. Department of Energy [20]. The position and momentum of particles are explicitly described according to Newton's laws:

$$\frac{dX^{(i)}(t)}{dt} = V^{(i)}(t), \tag{1}$$

$$m^{(i)}\frac{dV^{(i)}(t)}{dt} = F_T^{(i)}(t) = m^{(i)}g + F_d^{(i\in k,m)}(t) + F_c^{(i)}(t), \tag{2}$$

$$I^{(i)}\frac{d\Omega(t)}{dt} = T^{(i)}(t), \tag{3}$$

where $X^{(i)}$ is the particle position of the ith particle within the domain at time t, $V^{(i)}$ is the velocity, $\Omega(t)$ is the angular velocity of the ith particle, $m^{(i)}$ is the particle mass, and g is gravity. $F_c^{(i)}$ is the net contact force, $F_T^{(i)}$ is the sum of the forces acting on the ith particle, and $F_d^{(i\in k,m)}$ is the total (viscous and pressure) drag force acting on particle i if the mth solid phase is located within the kth cell. $T^{(i)}$ is the sum of all torques acting on the ith particle, and $I^{(i)}$ is the moment of inertia. Particle contacts are modeled using the soft-sphere method, which uses the spring-dashpot approach that has been rigorously validated in a series of studies [20,21]. In this soft-sphere approach, the overlap between particles is simulated by a series of springs and dashpots in the normal and tangential directions. The dashpot is used to model the loss of kinetic energy during inelastic collisions, while the spring models the rebound of a particle that is in contact with another. Both dashpot and spring are described with dampening and stiffness coefficients in both the tangential and normal directions. In the DEM, each solid phase is described by a distinct diameter and density. Unless specified, particles have a density of 1050 kg/m^3 and a particle-particle friction of 0.53, motivated by values from geophysical flows. The restitution coefficient has been shown to have a negligible impact on stresses (see Gu *et al.* [18]) and was set at 0.6 (inspired by the value of natural geological mixtures [22]) between all phases. Particle assemblies are described as follows: (1) monodisperse, (1a) with variable solid density (500, 1050, and 2500 kg/m^3), (1b) with a diameter of 1.75, 2, 3, 4, and 5 mm, (1c) with particle friction of (0.09, 0.25, 0.8), (1d) density biphasic (density pairs of 1050–2500,

500–1050, and 500–2500 kg/m^3, (1e) friction biphasic (0.09–0.53, 0.25–0.53, 0.53–0.8, and 0.25–0.8), (2) polydisperse, (2a) bidisperse (1.75–5, 2–5, 3–5, and 4–5 mm), and (2b) tridisperse (5–3–2 and 5–4–2 mm). Each size distribution can be analyzed using the polydispersity parameter based on their radii r: $\delta = \frac{\sqrt{\langle \Delta r^2 \rangle}}{\langle r \rangle}$ and the skewness parameter: $S = \frac{\langle \Delta r^3 \rangle}{\langle \Delta r^2 \rangle^{\frac{3}{2}}}$, which measures the spread and shape of the particle size distribution (PSD), respectively [18]. In the equations, $\Delta r = r - \langle r \rangle$ and the moment of Δr and r and are defined as $\langle \Delta r^n \rangle = \int \Delta r^n P(r) dr$ and $\langle r^n \rangle = \int r^n P(r) dr$, respectively. The mean particle diameter chosen as the volume-mean diameter (D_{43}) is defined as follows:

$$D_{43} \equiv \frac{\sum_{i=1}^{N} d_i^4}{\sum_{i=1}^{N} d_i^3}, \tag{4}$$

where N is the total number of particles and d_i is the diameter of particle i. In our simulations, the particle stiffness is set at $k_n = 10^4 Pd$ to ensure particle interactions fall in the hard contact regime [23]. Assemblies of grains were placed in a periodic box with fixed volume and vertically bounded by a rough bottom static plate and a moving top rough plate that imposed a confining pressure and moved at a set velocity in one direction. Roughness is generated by fixing the relative position of particles based in a monolayer. A second rough plate of particles was created away from the plates to prevent slip at high top plate velocities and to ensure a constant shear rate across the bed in the simple shear simulations [Fig. 1(a)]. Each simulation consists of an initial phase where the bed is compacted and presheared, followed by a phase where the top plate reaches the set velocity and that velocity is held constant. Once it reaches a steady state, the particle velocity, contact forces, diameter, density, and friction are exported and used for postprocessing using the coarse-graining (CG) method. For each set, 22 simulations were run at a constant confining pressure of 2 kPa and varying top plate velocities (from 0.0001 to 32 m/s) to span the quasistatic to inertial-collisional flow regimes. The simple shear simulations were conducted without a gravity field. In addition, a series of simulations were performed using different particle size distributions: monodisperse (5 mm), bidisperse (2–5 mm), and tridisperse (2–3–5 mm). These simulations were carried out on various geometries: (a) a sloped surface with the influence of gravity, resulting in concave flows, and (b) simple shear with gravity, resulting in an exponential-like velocity profile across the bed [Fig. 1(b)], thereby inducing a vertical shear gradient and subsequent nonlocal behavior. Similar to the gravity-free simple shear simulations, only steady-state data were analyzed.

B. Coarse graining

The formulation of accurate continuum models of granular flows requires the use of experimental or numerical data (i.e., from DEM), which are by nature made of discrete entities [24–26]. To this end, micro-macro transition methods are used to obtain continuum fields (such as density, momentum, stress) from discrete data of individual elements (positions, velocities, orientations, interaction forces). The coarse-graining method allows us to calculate continuum fields by applying a local smoothing kernel, coarse-graining function, with a well-defined smoothing length, i.e., coarse-graining scale, that automatically generates fields satisfying the continuum equations [27]. In this study, we use the Lucy coarse-graining function:

$$\psi(\mathbf{r}) = \frac{105}{16\pi c^3}\left[-3\left(\frac{a}{c}\right)^4 + 8\left(\frac{a}{c}\right)^3 - 6\left(\frac{a}{c}\right)^2 + 1\right] \text{ if } a = \frac{|\mathbf{r}|}{c} < 1 \text{ otherwise } 0, \tag{5}$$

where the cutoff lengthscale $c = 2 * D_{43}$ and the coarse-graining scale $w = 0.75 * D_{43}$. We ran the coarse-graining analysis away from the boundaries, with an offset of $1.5 * c * w + 0.5 * d_{\max}$. From the coarse-graining analysis, we calculate the macroscopic stress tensor:

$$\sigma(r,t) = \sigma^k(r,t) + \sigma^c(r,t), \tag{6}$$

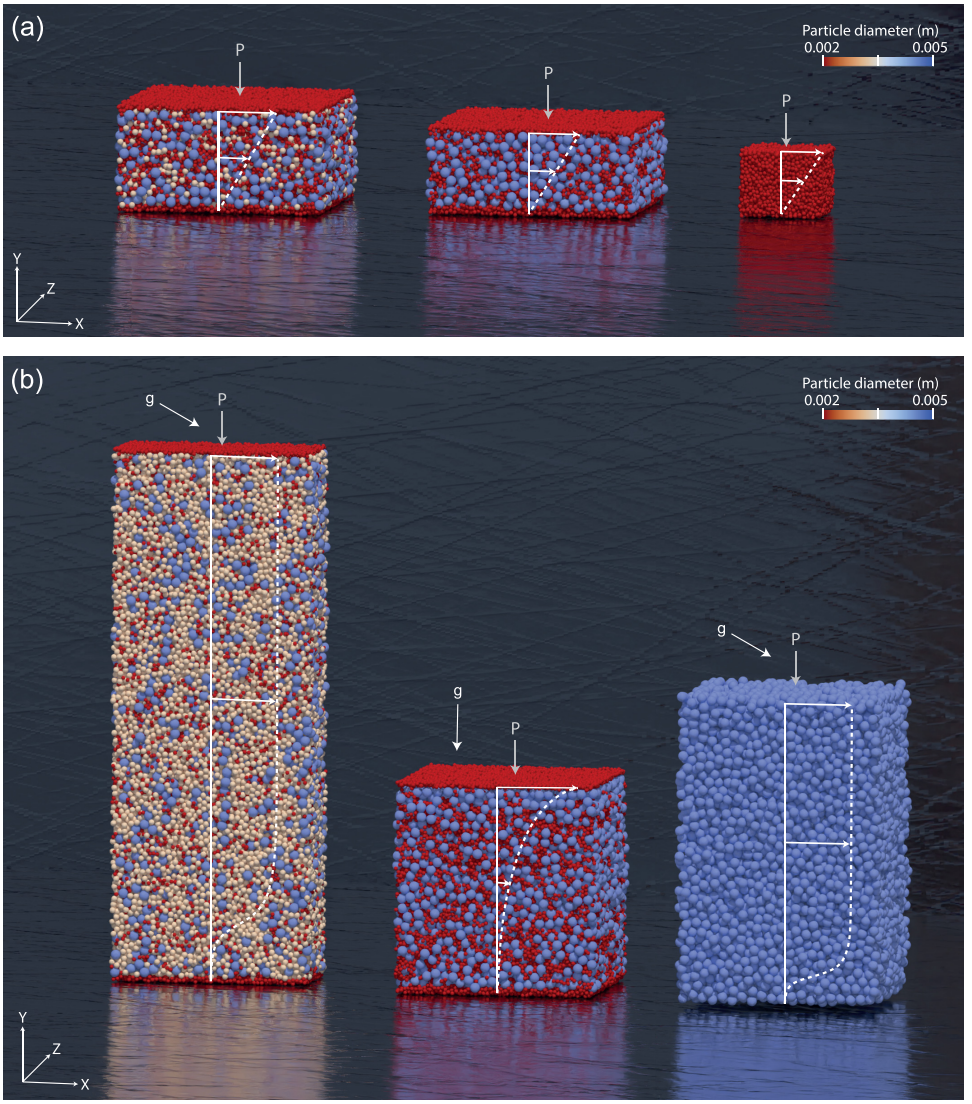

FIG. 1. Planar shear geometry for local (linear velocity profile) and nonlocal (nonlinear velocity profile) rheology tests. (a) Simple shear for tridisperse, bidisperse, and monodisperse particle size distributions (left to right) devoid of gravity field. (b) Concave flows created using a 60° slope with gravity. All planar shear tests consist of an imposed confining pressure of 2 kPa and an imposed velocity V_x of 0.0001–32 m/s.

where the kinetic tensor depends on particle velocity fluctuations and the contact tensor depends on the contact forces. The full description of the tensors is provided by Breard *et al.* [28].

The granular friction coefficient is calculated from the 2D version of the stress tensor in combination with the pressure using all three contributions, which is the more appropriate approach for plane shear flow setups [26],

$$\mu = \frac{|\sigma^D|}{P}, \tag{7}$$

where

$$\left|\sigma^{D}\right| = \sqrt{0.5\sigma_{ij}^{\prime D}\sigma_{ij}^{\prime D}}. \tag{8}$$

All the data presented in this manuscript are for beds that are yielding (i.e., where a shear rate is measurable). The average normal stress or solid pressure in the system is calculated as the trace of the 3D stress tensor:

$$P = \frac{1}{3}\,\mathrm{tr}(\sigma), \tag{9}$$

$$T_g = \frac{\mathrm{tr}\left(\sigma^{k}\right)}{3\rho}. \tag{10a}$$

The above equation introduced by [26] gives the same results as the more intuitive approach:

$$T_{\mathrm{g\ lammps}} = \frac{2E_{\mathrm{kin}}}{N_{\mathrm{DOF}}} \tag{10b}$$

with

$$E_{\mathrm{kin}} = \sum_{i=1}^{N} \frac{1}{2} m_i (v_i - \bar{v})^2. \tag{10c}$$

N_{DOF} is the total number of degrees of freedom for those atoms, given by the product $N*n$, where N is the number of atoms and n is the degree of freedom (=3 for 3D simulations and using the magnitude of the particle velocity). m_i is the particle mass with velocity v_i. $\bar{v}$ is the average velocity of the N atoms.

We use the approach described by Eqs. (10b) and (10c) to extract the granular temperature from our simulations. First, we decompose the domains in n vertical slices with thickness $<0.1D_{43}$ that ensures scale independence. Second, we calculate the granular temperature in each vertical slice. Finally, we either average the granular temperature vertically to obtain depth-averages or we recalculate the granular temperature at a resolution matching that of the coarse-graining approach ($=1.5*D_{43}$) to look at height-variant granular rheology.

For all planar shear simulations, with and without gravity, the data presented in the manuscript are obtained by spatial and temporal averaging of the CG fields across the whole bed, excluding the cells located at a distance of three mean particle diameter from the boundaries to avoid any of their effects. The CG postprocessing analysis provides data along the entire bed where gradients of all properties exist. The data presented, unless explicitly specified, represent the depth-averaged coarse-grained flow fields.

C. Empirical function fitting

Once the flows reached steady state, we exported discrete data at 10 Hz that were postprocessed using the CG method to calculate instantaneous fields. For each simulation, the fields were space- and time-averaged over a time-window of 2–4 s.

We show that the standard $\mu(I)$ and a common form of $\phi(I)$ hold in all simple shear numerical simulations, but with the fitting parameters dependent on the particle size, density, and surface friction dependence,

$$\mu = \mu_1 + \frac{\mu_2 - \mu_1}{1 + I_0/I}, \tag{11}$$

$$\phi = \phi_c - \alpha I^{\gamma}. \tag{12}$$

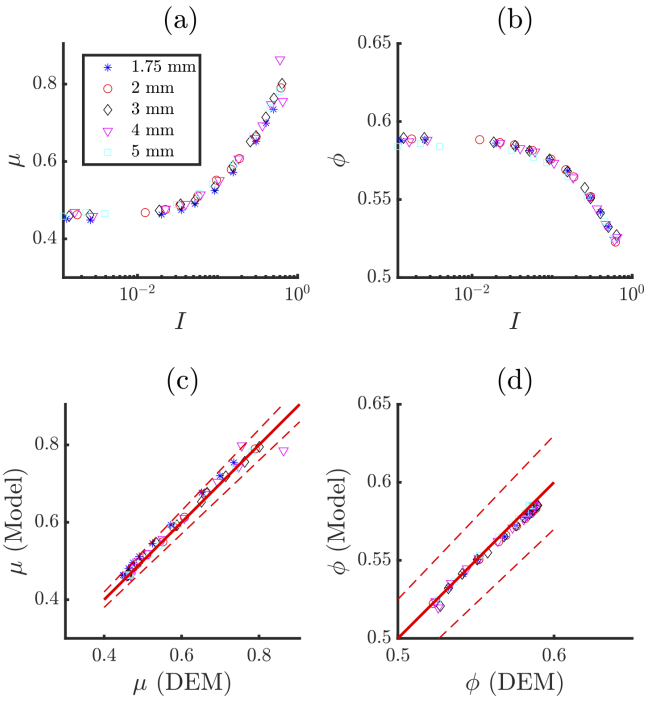

FIG. 2. Stress ratio μ (a) and concentration ϕ (b) as a function of the inertial number I for monodisperse mixtures. Modeled stress ratio (c) and concentration (d) against numerical simulations. Dotted red lines are the 95% confidence interval for the linear fitting. The data are derived from planar simple shear simulations devoid of a gravity field.

III. RESULTS

A. Monodisperse simulations in simple shear

1. Monodisperse simple shear, varying particle size

First we perform a series of simple shear cell simulations with constant particle size to find the particle size dependence of the parameters μ_1, μ_2, I_0 in Eq. (11), and ϕ_c, α, γ in Eq. (12).

The parameters were found to be independent of particle size within the size range considered in this study, where the maximum size ratio investigated is 2.9. The fit was conducted with the 5 mm data, and the fitted model parameters were used to validate the size-independent assumption in Fig. 2. For the friction equation, the fitted parameters are

$$\mu_1 = 0.4607, \tag{13}$$

$$\mu_2 = 1.1223, \tag{14}$$

$$I_0 = 0.6253. \tag{15}$$

For the volume fraction, the fits are

$$\phi_c = 0.5858, \tag{16}$$

$$\alpha = 0.0939, \tag{17}$$

$$\gamma = 0.8180. \tag{18}$$

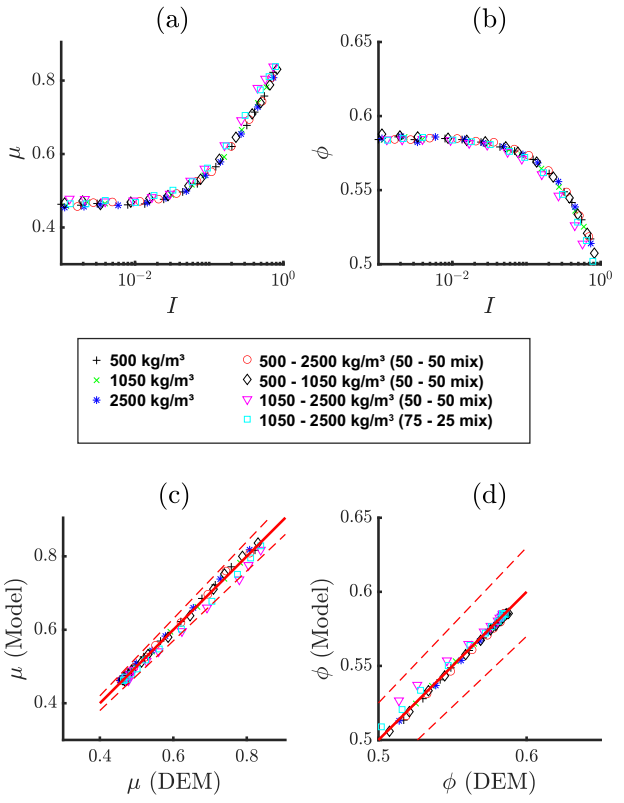

FIG. 3. Stress ratio μ (a) and concentration ϕ (b) as a function of the inertial number I for density mixtures. Modeled stress ratio (c) and concentration (d) against numerical simulations. The dotted red lines are the 95% confidence interval for the linear fitting. All data were obtained from simulations without gravity with a planar simple shear geometry.

The collapse of stress ratio and concentration data with the inertial number is in line with the classic $\mu(I)$-rheology [12,29].

2. Simple shear, varying particle density

To investigate the rheology of biphasic mixtures where particles have a monodisperse grain-size distribution but varying particle density, we perform simple shear cell numerical simulations. For simulations with a constant particle density, or density mixtures, the $\mu(I)$ and $\phi(I)$ curves all fall onto the same curve (Fig. 3), as long as the volume-weighted density is used in the inertial number calculation.

If ϵ is the volume weighting of the particle phase with density $\rho = \rho_1$ in the particle mixture, then $\rho_{\text{mix}} = \epsilon\rho_1 + (1-\epsilon)\rho_2$.

3. Simple shear, varying particle surface friction coefficient

Simple shear numerical simulations were performed with (a) particles of the same size and density, but varying particle-particle friction coefficients and (b) particles of the same density but different diameters. The particle-particle friction coefficient varied from values as low as 0.09 up to 0.8.

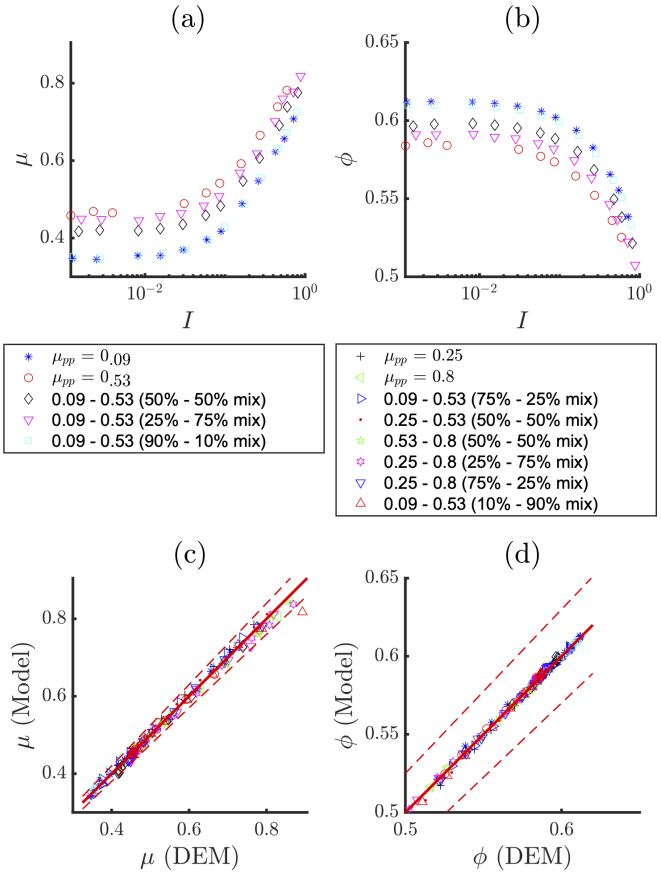

FIG. 4. Stress ratio μ (a) and concentration ϕ (b) as a function of the inertial number I for mixtures with varying particle-particle friction μ_{pp}. Modeled stress ratio (c) and concentration (d) against numerical simulations. Dotted red lines are the 95% confidence interval for the linear fitting. The data come from planar simple shear simulations devoid of a gravity field.

As expected, the stress ratio μ and ϕ are strongly dependent on the particle-particle friction coefficient μ_{pp} (Fig. 4) and can be scaled with the inertial number in the following way:

$$\mu_1^{\text{pp}} = 0.4674 - 0.2199\exp(-6.1427\mu_{\text{pp}}), \tag{19}$$

$$\mu_2^{\text{pp}} = 1.0806, \tag{20}$$

$$I_0^{\text{pp}} = 0.7306 - 0.2701\mu_{\text{pp}}, \tag{21}$$

and

$$\phi_c^{\text{pp}} = 0.5826 + 0.0457\exp(-4.4828\mu_{\text{pp}}), \tag{22}$$

$$\alpha^{\text{pp}} = 0.0952, \tag{23}$$

$$\gamma^{\text{pp}} = 0.9249 - 0.2098\mu_{\text{pp}}. \tag{24}$$

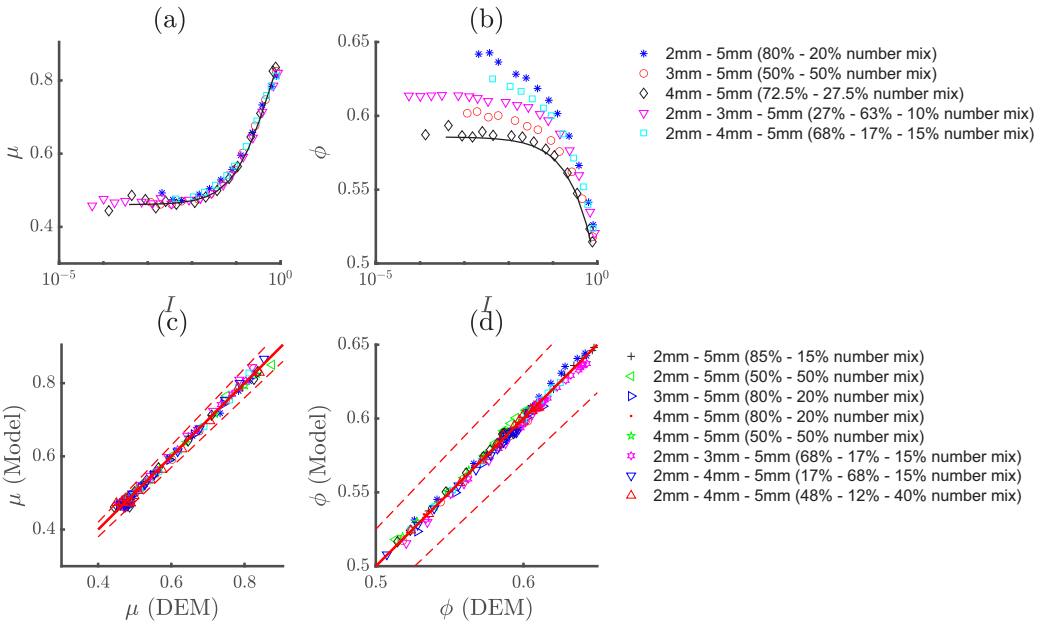

FIG. 5. Stress ratio μ (a) and concentration ϕ (b) as a function of the inertial number I for polydisperse size mixtures. Modeled stress ratio (c) and concentration (d) against numerical simulations. The dotted red lines are the 95% confidence interval for the linear fitting. The black lines in (a) and (b) represents the $\mu(I)$ and $\phi(I)$ fits from Eqs. (31)–(36), using only the first term of the RHS.

The $\mu(I)$ coefficients for the particle mixtures were found to be volumetrically related to the coefficients of individual populations denoted a and b. That is,

$$\mu_1^{\text{mix}} = (1-\epsilon)\mu_1^b + \epsilon\mu_1^a, \tag{25}$$

$$\mu_2^{\text{mix}} = (1-\epsilon)\mu_2^b + \epsilon\mu_2^a, \tag{26}$$

$$I_0^{\text{mix}} = (1-\epsilon)I_0^b + \epsilon I_0^a. \tag{27}$$

For the particle mixtures, the $\phi(I)$ coefficient ϕ_c was found to be volumetrically related to the individual coefficients of the two particle populations, namely a and b, but the α and γ coefficients were not found to be a function of particle friction (Fig. 5). Instead, they are only a function of particle diameter, as expressed in Eqs. (17) and (18). That is,

$$\phi_c^{\text{mix}} = (1-\epsilon)\phi_1^b + \epsilon\phi_1^a, \tag{28}$$

$$\alpha^{\text{mix}} = \alpha^b = \alpha^a, \tag{29}$$

$$\gamma^{\text{mix}} = \gamma^b = \gamma^a, \tag{30}$$

B. Polydisperse simulations in simple shear

As demonstrated by [18], the friction and dilatancy of polydisperse granular-size mixtures are a function of the skewness and polydispersity parameters (see the Methods section for definition). In

TABLE I. Fitting parameters for the polydisperse mixtures.

		C_1^i	C_2^i	C_3^i
$i = a$	μ_1	−0.002243	0.03100	0.003543
$i = b$	μ_2	−0.09007	0.3527	−0.7073
$i = c$	I_0	−0.1926	0.6418	−1.040
		D_1^i	D_2^i	D_3^i
$i = a$	ϕ_c	0.0002977	0.05430	0.1195
$i = b$	α	−0.007443	0.04073	0.08477
$i = c$	γ	0. 006517	−0.5353	−0.1435

addition, we define $\epsilon_{S/M/L}$ as the volume fraction of the small/medium/large phase, denoted a, b, and c, respectively. Therefore, the friction law coefficients of Eq. (11) can be written as follows:

$$\mu_1^{\text{mix}} = \mu_1 + C_1^a + C_2^a\delta + C_3^a S\delta^2, \tag{31}$$

$$\mu_2^{\text{mix}} = \mu_2 + C_1^b + C_2^b\delta + C_3^b S\delta^2, \tag{32}$$

$$I_0^{\text{mix}} = I_0 + C_1^c + C_2^c\delta + C_3^c S\delta^2, \tag{33}$$

where $C_{1,2,3}^i$ are constants (Table I).

We calculated the MAPE (mean average percentage error) for the fitting of μ using all terms, as well as for the μ fitting using only the first term on the right-hand side. The results were 1.1% (all terms) and 1.9% (first term only). These values are averages over the different curves shown in Fig. 5(a). The variation in the $\mu(I)$ model suggests a very mild dependency of the μ parameters on grain-size, as observed previously in Ref. [18].

Similarly, the dilatancy law [Eq. (12)] can be written following the work of Ref. [18] to account for the particle size distribution of the granular mixture:

$$\phi_c^{\text{mix}} = \phi_c + D_1^a + D_2^a\delta + D_3^a S\delta^2, \tag{34}$$

$$\alpha^{\text{mix}} = \alpha + D_1^b + D_2^b\delta + D_3^b S\delta^2, \tag{35}$$

$$\gamma^{\text{mix}} = \gamma + D_1^c + D_2^c\delta + D_3^c S\delta^2, \tag{36}$$

where $D_{1,2,3}^{a,b,c}$ are constants presented in Table I. To assess the need to include other terms in Eqs. (34)–(36), we calculated the MAPE for the fitting of ϕ using all terms, as well as when considering only the initial term on the right-hand side (RHS). The MAPE values were 0.3% for all terms and 3.0% for the first term alone. These percentages are averaged across the various curves shown in Fig. 5(b). As indicated by the change in MAPE values by an order of magnitude and the black line in Fig. 5, which represents the fitting of ϕ using only the first term, it is evident that size dispersity should be considered. The noise in the data cannot account for the differences we observe between the mixtures.

IV. DISCUSSION

In the present study, we explored the biphasic mixtures of grains with different particle-particle friction coefficients, densities, and size distributions, and we found the inertial number is indeed capable of capturing the evolution of the stress ratio μ and dilatancy ϕ provided that one accounts for the contribution of each particle phase by volume using the D_{43} as the characteristic particle lengthscale in the system. Although our research is limited to particles within the hard contact regime, it carries significant relevance for the majority of both natural and industrial granular flows.

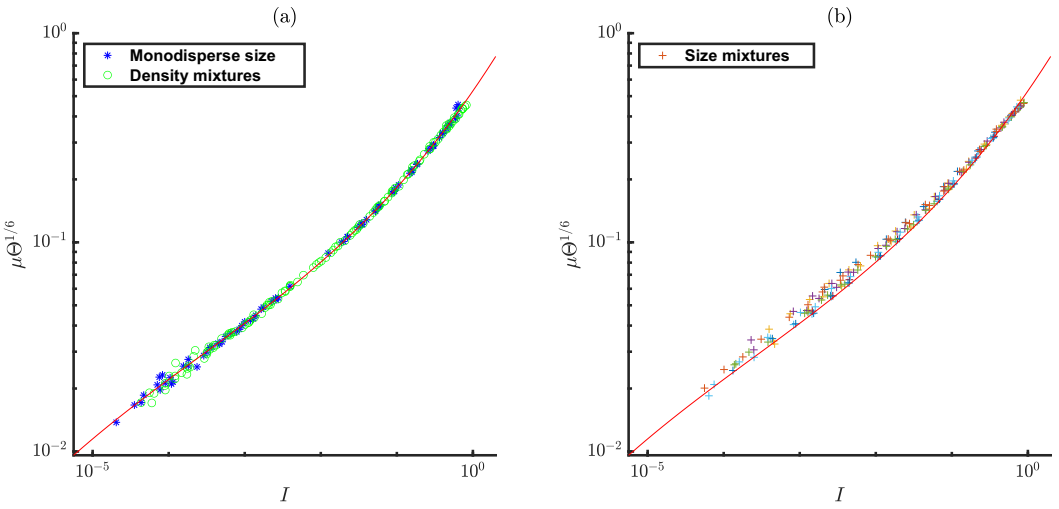

FIG. 6. Power-law scaling as defined by Kim and Kamrin [19] $\mu\Theta^{1/6} = f(I)$ for monodisperse and density mixtures (a) and size mixtures (b).

In the past decades, the kinetic theory (KT) originally developed for gases, has been adapted to describe the frictional regime of granular flows [30–33], but this modified KT has yet to be adapted to describe polydisperse mixtures. Expanding on the KT that characterizes the solid pressure in relation to the granular temperature, Kim and Kamrin [19,34] have recently implemented a power-law scaling for the stress ratio. This scaling correlates with the inertial number and the dimensionless granular temperature, defined as $\Theta \equiv \rho_s T/P$. Granular temperature has proven to be a critical parameter in the development of constitutive models for flows that exhibit both liquid- and solidlike behaviors [35].

In light of these findings, we investigate a potential scaling $\mu(I, \Theta)$ across all the size distributions. We observe that "heating" the material (endogenous mechanical vibrations), or increasing the granular temperature, tends to weaken (or soften) the material, and it follows that $\mu\Theta^p = f(I)$, where p equals $1/6$ [as shown in Fig. 6(a)].

Contrary to Kim and Kamrin's approach [19], which relied solely on the streamwise velocity component to calculate granular temperature and the vertical component to calculate solid pressure, we employed all three components of stress [Eqs. (9) and (10a)] in the calculation of the granular temperature and the solid pressure. In addition, we also used the deviatoric shear rate and deviatoric shear stress.

Our data are represented by the following polynomial expression:

$$\ln\left(\mu\Theta^{1/6}\right) = 0.0011\ln^3(I) + 0.0280\ln^2(I) + 0.5071\ln(I) - 0.5024. \tag{37}$$

While the monodisperse and density mixture data fall perfectly on the same curve, the data from polydisperse simulations do not coincide with the monodisperse data across the spectrum of quasistatic to inertial/collisional regimes [see Fig. 6(b)].

We explored a variety of scalings to collapse the data on a single master curve. Kim and Kamrin [19] introduced the scaling $\mu(I, \Theta)$, which successfully removed the rheological dependence on ϕ. Notably, the successful alignment of $\mu = f(I)$ data from monodisperse simulations across flow geometries in studies by [19,34] allowed them to eliminate the concentration dependency in their scaling and continuum model. However, this method is not suitable for polydisperse mixtures. This is evident as the data for ϕ and μ do not align due to the polydispersity, as seen in Fig. 1 of the Supplemental Material [36]. Since this alignment is not observed in our data, we explored ways to use the solid concentration ϕ to make our data collapse upon one curve. As a result, we

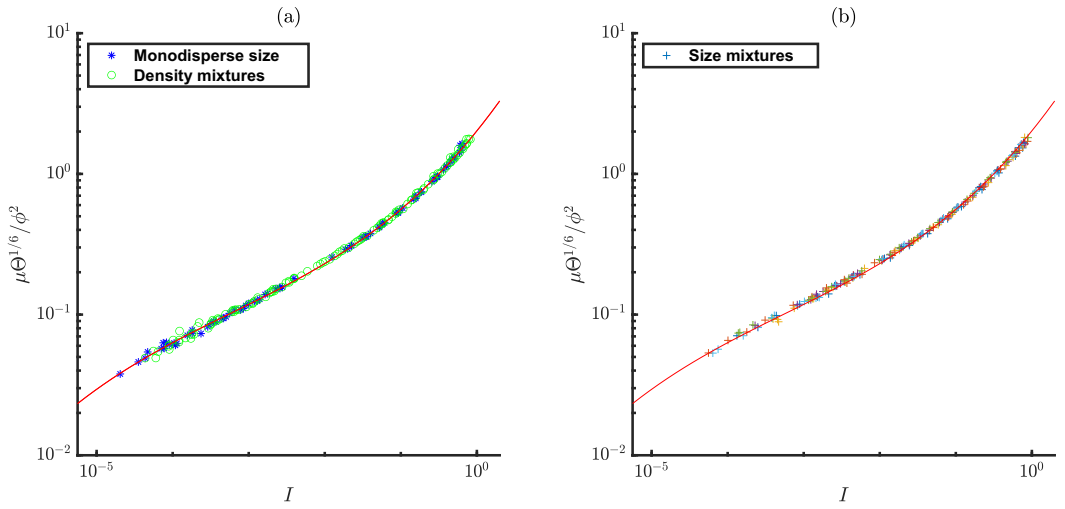

FIG. 7. Modified power-law scaling $\frac{\mu\Theta^{1/6}}{\phi^2} = f(I)$ for monodisperse and density mixtures (a) and size mixtures (b). The red line is the same in both plots.

derived a modified power-law scaling, $\mu(I, \Theta, \phi)$, fitted first to our monodisperse data. The ensuing formulation is presented in Fig. 7(a):

$$\ln\left(\mu\Theta^{1/6}/\phi^2\right) = 0.0023\ln^3(I) + 0.0505\ln^2(I) + 0.6466\ln(I) + 0.8356. \tag{38}$$

Our fitting approach, derived from the monodisperse simple shear simulations, enables a well-aligned collapse of polydisperse simple shear simulation data [Fig. 7(b)]. The successful collapse of all simple shear data onto a single line indicates that the stress ratio μ can be predicted using solely dimensionless parameters—the inertial number I, solid concentration ϕ, and scaled granular temperature Θ. Using a sensitivity analysis, we determined that an exponent value of 2 for the ϕ term provides the best fit (see Table 1 of the Supplemental Material [36]). However, the physical rationale behind the selection of values for the two exponents remains an open question. We deduce that the exponent $p = \frac{1}{6}$ is a universal characteristic, independent of specific material properties and definitions of stress, pressure, or granular temperature. Furthermore, by employing the deviatoric shear stress and deviatoric shear rate, as well as the full trace of the kinetic stress tensor to calculate the pressure and granular temperature (in a manner similar to [26]), our methodology diverges from that of [19] to provide a comprehensive description of the system. We tested whether using a single component of stress (x-direction for granular temperature and y-component in the pressure calculation) impacted our findings. As shown in Figs. 2 and 3 of the Supplemental Material [36], the necessity of employing the concentration to scale the stress ratio data appears to be unaffected by the components of granular temperature or pressure used. We also investigated whether the definition of granular temperature could be the reason for the data's noncollapse when plotting them as in Ref. [19]. Instead of calculating the mean velocity using the mixture velocity, we determined the mean velocity for each phase. This approach resulted in similar trends where both monodisperse and polydisperse data did not collapse without including the term ϕ^2 in the scaling.

The collapse of our monodisperse and polydisperse results has major implications. Before, the stress ratio needed to be defined based on various empirical fits to describe the size and density mixtures. Instead, Fig. 7 suggests that a single empirical polynomial law combined with conservation of mass (to describe ϕ) predicts the stress ratio for all situations investigated. Consequently, the

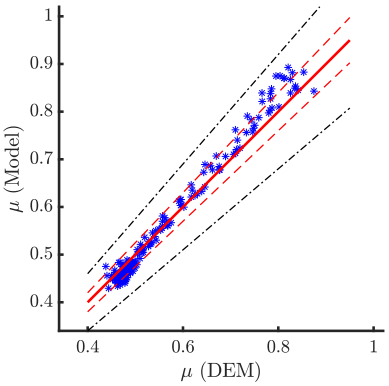

FIG. 8. Modified power-law scaling of the stress ratio μ(Model) predictions against numerical simulation data μ(DEM) for all mixtures. The red and black lines indicate the 5% and 15% error, respectively.

following scaling describes the flow rheology:

$$\frac{\mu\Theta^{1/6}}{\phi^2} = f(I). \tag{39}$$

Using this approach, we predict the stress ratio of size, density, and friction of mixtures investigated and show that it works very well for $\mu < 0.75$ (Fig. 8). The large sensitivity at large inertial numbers with friction that is up to 15% higher than predicted by Eq. (38) could be explored in future work using a fitting function of higher order.

In our final analysis, we examine the rheology of both monodisperse and polydisperse grain-size distributions within a variety of flow configurations. These configurations encompass thick flows featuring vertical shear gradients (evidenced by an exponential velocity profile) and subject to gravity, thin flows devoid of gravity (indicated by a linear velocity profile), and flows moving down a slope (characterized by a concave velocity profile; see Fig. 1). We illustrate the vertical gradients in flow properties across all three simulation setups [monodisperse, bidisperse, tridisperse, Figs. 9(a)–9(c)]. The results show that regions of the flow with minimal shear benefit from the diffusion of granular temperature originating from areas with significant shear. These low-shear regions (shaded blue in Fig. 9), which have an inertial number less than 10^{-2}, correspond to a friction coefficient lower than the static friction coefficient μ_1 of the mixture. This nonlocal behavior is primarily driven by granular heating, which induces "fluidity" in regions that would otherwise remain stationary. This phenomenon is observed in areas where the solid fraction surpasses the ϕ_c value.

When considering the depth average, flows displaying nonlocal effects exhibit a friction coefficient lower than what is predicted by their simple shear analogs [Fig. 10(a)]. This indicates that the strategy of accounting for size dispersity via a "mixture rule" in the $\mu(I)$-rheology law, as outlined in Eqs. (31)–(36), is not applicable when nonlocal effects become dominant. Therefore, we aim to investigate a more generalized rheological model that takes nonlocal effects into account. Frictional weakening is observed in low shear regions where the flow is either in the intermediate or quasistatic regime (with $I < 0.1$), as clearly depicted in Figs. 9(a)– 9(c) and Fig. 10(a). In these areas, particle vibrations (measured through scaled granular temperature Θ) are efficiently propagated through the contact network resulting in an increase of the local (Fig. 9) and depth-averaged granular temperature for a given inertial number [Fig. 10(b)]. As demonstrated by [19], Θ is pivotal in understanding the reduction of the friction coefficient, a process we refer to as granular heating, which leads to frictional weakening [Figs. 10(a)–10(c)]. Therefore, we examine if the relation $\mu\Theta^p = f(I)$ proposed by [19] based on monodisperse simulations can collapse our data. However,

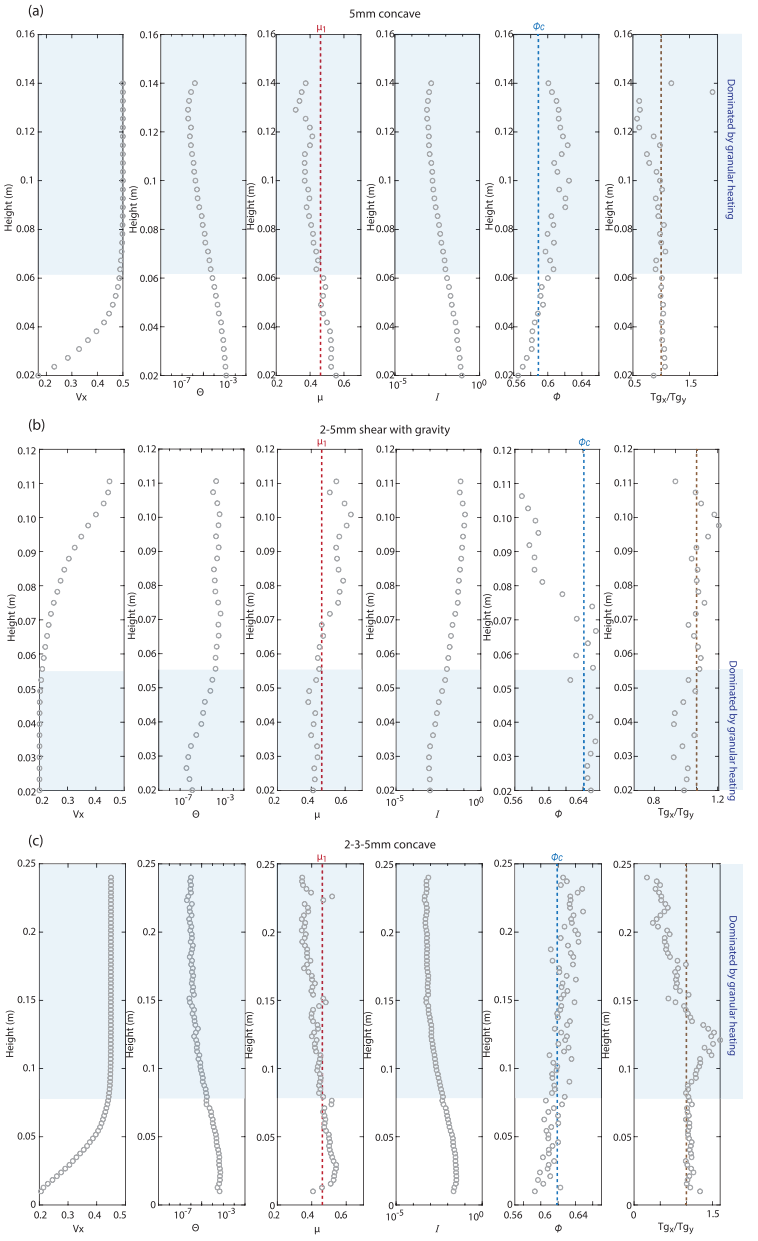

FIG. 9. Vertical profiles of streamwise velocity Vx, dimensionless granular temperature Θ, friction coefficient μ, inertial number I, solid concentration ϕ, and ratio of granular temperature Tg_x/Tg_y for one monodisperse 5 mm simulation (a), one 2–5 mm bidisperse simulation (b), and one 2–3–5 mm simulation setup (c). The vertical red dashed line represents μ_1. The blue vertical dashed lines represent ϕ_c and the brown dashed line represents a ratio of granular temperature of 1. The shaded blue regions highlight the portion of the flows where the friction coefficient is lower than the μ_1 value and where nonlocal rheology dominates.

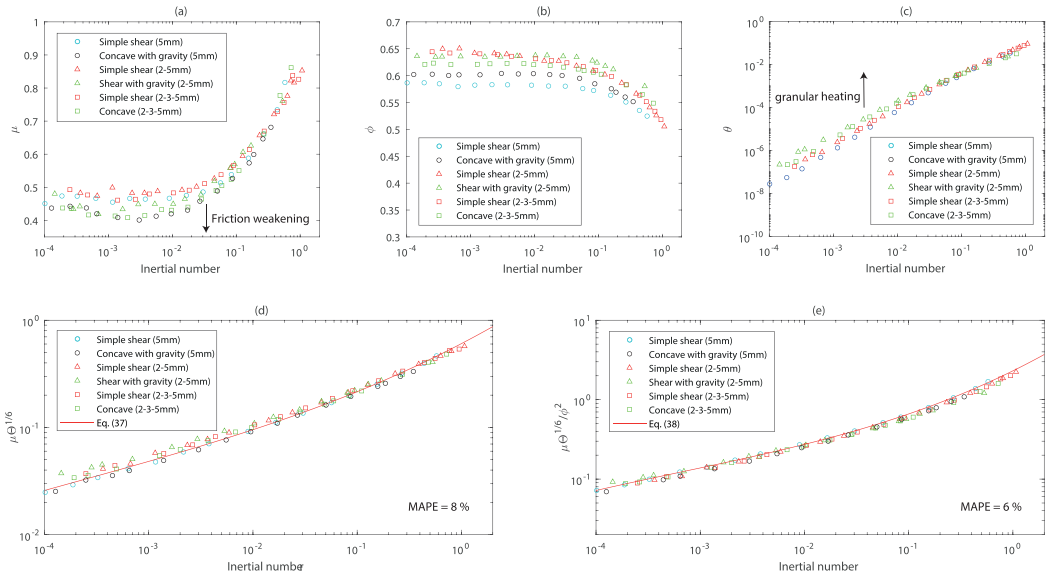

FIG. 10. Stress ratio μ (a), solid concentration (ϕ) (b) and granular temperature Θ (c) as a function of the inertial number. Power-law scaling $\mu\Theta^{1/6} = f(I)$ (d) and modified power-law scaling $\frac{\mu\Theta^{1/6}}{\phi^2} = f(I)$ (e) for monodisperse and polydisperse mixtures in simple shear, concave and shear with gravity flow geometries. The red lines are the fits derived from the monodisperse simple shear simulations.

our results collected from different flow geometries and particle assembly (size dispersity) do not align onto a singular curve [Fig. 10(d)].

Instead, we find better alignment of the nonlocal data on a master curve when using the scaling $\mu(I, \Theta, \phi)$, fitted with Eq. (38), derived from local shear simulations [Fig. 10(e)]. Therefore, the latter scaling effectively encapsulates the nonlocal behavior emerging from the spatial diffusion of granular temperature in polydisperse granular mixtures, and it allows us to unite with a power-law scaling the rheology of monodisperse and polydisperse grain-size mixtures across flow geometries.

To integrate our findings into a continuum framework, a structured methodology is recommended. First, it is essential to conduct simple shear simulations to determine parameters like μ, Θ, ϕ, and I. After determining these parameters, Eq. (38) can be fitted to the DEM data. The new continuum model should include an equation for estimating the granular temperature and another for ϕ, in addition to other conventional metrics such as pressure. Armed with these components, the empirical power-law rheology, encapsulated by Eq. (38), can be employed to compute μ. This, in turn, aids in defining the viscosity for the continuum model. This methodology markedly deviates from the traditional $\mu(I)$ model, aligning more with a modified kinetic theory approach. The primary outcome of our work demonstrates the sole need to run DEM simulations of monodisperse simple shear to derive the power-law scaling required for a specific set of particle properties (i.e., particle-particle friction). Importantly, any successful application of this rheological approach in a continuum framework requires that the spatial resolution of the continuum model be sufficient that grain properties are consistent throughout the averaging volume. For example, flows with large gradients in concentration would require addressing these varying properties (for instance with a resolved grid) while employing this rheological approach.

An alternative methodology could involve adopting the framework proposed by Ref. [37], which characterizes nonlocal behavior through a partial differential equation that governs the *granular fluidity* field, defined as $g = \frac{\dot{\gamma}}{\mu}$. Intriguingly, this granular fluidity is seemingly linked to two fundamental state variables: the granular temperature and the solid fraction, as suggested by Zhang

et al. [23]. A comparative analysis of kinetic theory, the granular fluidity concept, and the findings of our current study may unveil new, beneficial insights.

V. CONCLUSION

In this work, we have investigated the rheology of shear flows of dense, frictional granular media made of monodisperse, polydisperse, and biphasic (friction and density) particles. We observed the occurrence of well-known quasistatic, intermediate, and inertial/collisional regimes for all mixtures, with a strong dependence of the critical volume fraction ϕ_c on the skewness and polydispersity and the particle-particle friction of the media. We find that the inertial number scaling of the stress ratio remains valid as long as the volumetric contribution of the size (using the volume mean diameter D_{43}), density, and particle friction are accounted for in its definition. In addition, we bind the modified kinetic theory [30,32,38] to the $\mu(I)$-rheology by proposing an updated version of the power-law scaling introduced by Kim and Kamrin [19] to now account for polydisperse size distributions. We have established a new scaling for the stress ratio, which incorporates the dependence on the particle-particle friction coefficient and hinges on factors such as granular temperature, concentration, and the inertial number. Fundamentally, it encapsulates both local and nonlocal rheologies, which manifest as endogenous velocity fluctuations disperse spatially (through force chains) from areas of high granular temperature towards those with lower temperatures (granular heating). This mechanism, which dominates in the quasistatic and intermediate regime, results in an increase in granular temperature that is noticeably larger than the granular temperature predicted by $\Theta(I)$ from simple shear. The absence of granular heating in the gaseous regime at $I \gtrsim 0.1$ implies that nonlocality is enabled by the presence of force chains and suggests that the contact network, granular temperature diffusion, and nonlocality are intertwined. These findings emphasize the importance of investigating granular temperature and its diffusion, especially in contexts where nonlocal effects (i.e., large granular temperature gradients) are significant. This would enhance our understanding of polydisperse granular flows across various natural and industrial settings. Moreover, as natural granular media often exhibit rapid spatial changes in response to topographical shifts, further studies focusing on the transient behavior of granular media could provide a more holistic description of their rheology.

ACKNOWLEDGMENTS

E.C.P.B. was supported by a NERC Independent Research Fellowship (NE/V014242/1) and acknowledges the use of the ARCHER2 HPC facility and Talapas (University of Oregon) to run the computations. L.F. acknowledges funding from the Royal Society of New Zealand (Contract No. MAU1712). Financial support was provided by the National Science Foundation Grant No. EAR 1650382 to J.D. We thank P. J. Zrelak, Chongqiang Zhu, and Nathan Berry for valuable discussions about granular temperature.

[1] B. Sovilla, J. McElwaine, and A. Köhler, The intermittency regions of powder snow avalanches, J. Geophys. Res.: Earth Surf. **123**, 2525 (2018).

[2] R. M. Iverson, M. E. Reid, M. Logan, R. G. LaHusen, J. W. Godt, and J. P. Griswold, Positive feedback and momentum growth during debris-flow entrainment of wet bed sediment, Nat. Geosci. **4**, 116 (2011).

[3] O. Hungr, Rock avalanche occurrence, process and modelling, in *Landslides from Massive Rock Slope Failure* (Springer, Dordrecht, Netherlands, 2006), pp. 243–266.

[4] G. Lube, E. C. Breard, T. Esposti-Ongaro, J. Dufek, and B. Brand, Multiphase flow behaviour and hazard prediction of pyroclastic density currents, Nat. Rev. Earth Environ. **1**, 348 (2020).

[5] J. Dufek, The fluid mechanics of pyroclastic density currents, Annu. Rev. Fluid Mech. **48**, 459 (2016).

[6] P. D. Cole, A. Neri, and P. J. Baxter, Hazards from pyroclastic density currents, in *The Encyclopedia of Volcanoes* (Elsevier, Amsterdam, 2015), pp. 943–956.
[7] C. Huber, L. Ojha, L. Lark, and J. W. Head, Physical models and predictions for recurring slope lineae formed by wet and dry processes, Icarus **335**, 113385 (2020).
[8] J. Méndez Harper, G. McDonald, J. Dufek, M. Malaska, D. Burr, A. Hayes, J. McAdams, and J. Wray, Electrification of sand on titan and its influence on sediment transport, Nat. Geosci. **10**, 260 (2017).
[9] B. Andreotti, Y. Forterre, and O. Pouliquen, *Granular Media: Between Fluid and Solid* (Cambridge University Press, Cambridge, England, 2013).
[10] J. Estep and J. Dufek, Substrate effects from force chain dynamics in dense granular flows, J. Geophys. Res.: Earth Surf. **117**, F01028 (2012).
[11] H. J. Herrmann, J.-P. Hovi, and S. Luding, *Physics of Dry Granular Media* 350 (Springer Science & Business Media, Dordrecht, Netherlands, 2013), Vol. 350.
[12] P. Jop, Y. Forterre, and O. Pouliquen, A constitutive law for dense granular flows, Nature (London) **441**, 727 (2006).
[13] G. D. R. MiDi, On dense granular flows, Eur. Phys. J. E. Soft Matter **14**, 341 (2004).
[14] L. Staron, P.-Y. Lagrée, and S. Popinet, Continuum simulation of the discharge of the granular silo, Eur. Phys. J. E **37**, 5 (2014).
[15] L. Fullard, C. Davies, A. Neather, E. Breard, A. Godfrey, and G. Lube, Testing steady and transient velocity scalings in a silo, Adv. Powder Technol. **29**, 310 (2018).
[16] E. C. Breard, J. R. Jones, L. Fullard, G. Lube, C. Davies, and J. Dufek, The permeability of volcanic mixtures–implications for pyroclastic currents, J. Geophys. Res.: Solid Earth **124**, 1343 (2019).
[17] R. M. Iverson, Landslide disparities, flume discoveries, and Oso despair, Perspectives of Earth and Space Scientists **1**, e2019CN000117 (2020).
[18] Y. Gu, A. Ozel, and S. Sundaresan, Rheology of granular materials with size distributions across dense-flow regimes, Powder Technology **295**, 322 (2016).
[19] S. Kim and K. Kamrin, Power-law scaling in granular rheology across flow geometries, Phys. Rev. Lett. **125**, 088002 (2020).
[20] R. Garg, J. Galvin, T. Li, and S. Pannala, Open-source MFIX-DEM software for gas–solids flows: Part I–Verification studies, Powder Technol. **220**, 122 (2012).
[21] T. Li, R. Garg, J. Galvin, and S. Pannala, Open-source MFIX-DEM software for gas-solids flows: Part II–Validation studies, Powder Technol. **220**, 138 (2012).
[22] J. Dufek, J. Wexler, and M. Manga, Transport capacity of pyroclastic density currents: Experiments and models of substrate-flow interaction, J. Geophys. Res.: Solid Earth **114**, B11203 (2009).
[23] Q. Zhang and K. Kamrin, Microscopic description of the granular fluidity field in nonlocal flow modeling, Phys. Rev. Lett. **118**, 058001 (2017).
[24] T. Weinhart, C. Labra, S. Luding, and J. Y. Ooi, Influence of coarse-graining parameters on the analysis of dem simulations of silo flow, Powder Technol. **293**, 138 (2016).
[25] I. Goldhirsch, Stress, stress asymmetry and couple stress: from discrete particles to continuous fields, Granular Matter **12**, 239 (2010).
[26] T. Weinhart, R. Hartkamp, A. R. Thornton, and S. Luding, Coarse-grained local and objective continuum description of three-dimensional granular flows down an inclined surface, Phys. Fluids **25**, 070605 (2013).
[27] D. R. Tunuguntla, T. Weinhart, and A. R. Thornton, Comparing and contrasting size-based particle segregation models: Applying coarse-graining to perfectly bidisperse systems, Comput. Part. Mech. **4**, 387 (2017).
[28] E. C. P. Breard, L. Fullard, J. Dufek, M. Tennenbaum, A. Fernandez Nieves, and J. F. Dietiker, Investigating the rheology of fluidized and non-fluidized gas-particle beds: implications for the dynamics of geophysical flows and substrate entrainment, Gran. Matter **24**, 34 (2022).
[29] A. Fall, G. Ovarlez, D. Hautemayou, C. Mézière, J.-N. Roux, and F. Chevoir, Dry granular flows: Rheological measurements of the μ (i)-rheology, J. Rheol. **59**, 1065 (2015).
[30] D. Berzi, J. T. Jenkins, and P. Richard, Extended kinetic theory for granular flow over and within an inclined erodible bed, J. Fluid Mech. **885**, A27 (2020).

[31] C. K. Lun, S. B. Savage, D. Jeffrey, and N. Chepurniy, Kinetic theories for granular flow: inelastic particles in couette flow and slightly inelastic particles in a general flowfield, J. Fluid Mech. **140**, 223 (1984).
[32] V. Garzó and J. W. Dufty, Dense fluid transport for inelastic hard spheres, Phys. Rev. E **59**, 5895 (1999).
[33] J. T. Jenkins and S. B. Savage, A theory for the rapid flow of identical, smooth, nearly elastic, spherical particles, J. Fluid Mech. **130**, 187 (1983).
[34] S. Kim and K. Kamrin, A second-order non-local model for granular flows, Front. Phys. **11**, 1092233 (2023).
[35] C. Zhu, Y. Huang, and J. Sun, A granular energy-controlled boundary condition for discrete element simulations of granular flows on erodible surfaces, Comput. Geotech. **154**, 105115 (2023).
[36] See Supplemental Material at http://link.aps.org/supplemental/10.1103/PhysRevFluids.9.054303 for the table presenting the MAPE results, a Figure showing the concentration and friction relationship and the power-law scaling using Eqs. (37) and (38) using components similar to that of Ref. [19].
[37] K. Kamrin and G. Koval, Nonlocal constitutive relation for steady granular flow, Phys. Rev. Lett. **108**, 178301 (2012).
[38] C. K. Lun, Kinetic theory for granular flow of dense, slightly inelastic, slightly rough spheres, J. Fluid Mech. **233**, 539 (1991).